Computers in Biology and Medicine 183 (2024) 109283

Contents lists available at ScienceDirect

Computers in Biology and Medicine

journal homepage: www.elsevier.com/locate/compbiomed

Chance-constrained stochastic optimal control of epidemic models: A fourth moment method-based reformulation

Almudena Buelta, Alberto Olivares *, Ernesto Staffetti

Universidad Rey Juan Carlos, Camino del Molino 5, 28942, Fuenlabrada, Madrid, Spain

ARTICLE INFO

Keywords:
Stochastic optimal control
Chance constraints
Polynomial chaos expansions
Epidemic models
COVID-19

ABSTRACT

This work proposes a methodology for the reformulation of chance-constrained stochastic optimal control problems that ensures reliable uncertainty management of epidemic outbreaks. Specifically, the chance constraints are reformulated in terms of the first four moments of the stochastic state variables through the so-called fourth moment method for reliability. Moreover, a spectral technique is employed to obtain surrogate models of the stochastic state variables, which enables the efficient computation of the required statistics. The practical implementation of the proposed approach is demonstrated via the optimal control of two different stochastic mathematical models of the COVID-19 transmission. The numerical experiments confirm that, unlike those reformulations based on the Chebyshev–Cantelli's inequality, the proposed method does not exhibit the undesired outcomes that are typically observed when a higher precision is required for the risk level associated to the given chance constraints.

1. Introduction

Stochastic optimal control [1] is a powerful tool for decision-making under uncertainty. It is rooted in the principles of optimal control theory [2] and probability theory [3], providing a framework for optimizing the behavior of dynamic systems that are subject to uncertainties in the system dynamics or random disturbances. Utilizing a Bayesian probability-driven approach, it assumes that random noise with a known probability distribution influences the future evolution of the state variables' statistics. Moreover, stochastic optimal control develops the future trajectory of the controlled variables to achieve the desired control task, typically with some notion of minimum cost. However, real-world instances of stochastic optimal control problems often come with constraints that must be fulfilled. Specifically, probabilistic constraints, also known as chance constraints [4], are becoming increasingly relevant in various applications. These constraints limit the probability of certain undesirable events, thereby ensuring a determined level of performance or safety.

In particular, this paper delves into the application of chance-constrained stochastic optimal control to the uncertainty management of epidemic outbreaks. The model of disease spread is governed by differential equations with uncertain parameters [5]. Thus, it is a stochastic dynamical system, making chance-constrained stochastic optimal control techniques especially suitable for the control of the spread. The probability of severe outbreaks can be limited and public health interventions can be optimized by incorporating probabilistic constraints. Formulating an appropriate Chance-Constrained Stochastic Optimal Control Problem (CCSOCP) enables efficient resource allocation, such as vaccines or medical personnel, while minimizing the spread of the disease. It also aids in risk mitigation by quantifying uncertainty and incorporating it into decision-making processes, which contributes to mitigate the risks associated with public health decisions. Furthermore, the formulation of CCSOCPs can lead to more accurate and robust prediction models for disease spread, which can guide public health strategies and interventions. Notice that epidemics due to previously unknown or expected pathogens, or radically new strains, are Black Swan events, which are very difficult to predict and quantify probabilistically. In this sense, this paper assumes that the outbreak has already started and is recognized with some preliminary trend. Therefore, control over the future Black Swan events associated with the epidemic is not included in the scope of this work.

Various methodologies have been proposed to formulate and solve CCSOCPs. They include second-order cone programming [6], kernel density estimation [7], a combination of Polynomial Chaos Expansion (PCE) and subset simulation [8], statistical learning, [9] and Hilbert space embedding [10].

Specifically, with regard to the chance-constrained stochastic optimal control of epidemic outbreaks, the following recent works are noteworthy. The effects of isolation and weather on the control of the COVID-19 pandemic transmission have been investigated in [11].

* Corresponding author.
E-mail addresses: almudenajose.buelta@urjc.es (A. Buelta), alberto.olivares@urjc.es (A. Olivares), ernesto.staffetti@urjc.es (E. Staffetti).

https://doi.org/10.1016/j.compbiomed.2024.109283
Received 15 May 2024; Received in revised form 23 September 2024; Accepted 14 October 2024
Available online 24 October 2024

Different kinds of mathematical epidemic models have been employed in [12] to predict the dynamic behavior of the COVID-19 spread by means of the formulation and resolution of various inverse problems. A stochastic nonlinear Model Predictive Control (MPC) technique has been proposed in [13] to tackle the COVID-19 pandemic waves through nonpharmaceutical strategies. The optimal quarantine duration for COVID-19 uninfected people has been studied in [14]. Various social distancing strategies for the COVID-19 epidemic have been designed in [15] using an MPC approach. The optimal allocation of COVID-19 vaccines and tests has been addressed in [16]. A data-driven PCE approach has been presented in [17] to find the optimal vaccination and testing policies for the mitigation of the COVID-19 pandemic.

This paper presents a methodology for the reformulation of CCSOCPs, which ensures a reliable uncertainty management of epidemic outbreaks. In particular, the same data-driven PCE technique used in [17] is considered to obtain surrogate models of the optimal stochastic state variables. Nevertheless, the chance constraints are redefined using a different approach. In [17], the reformulation of the chance constraints is based on the Chebyshev–Cantelli's (CC) inequality. However, the bounds provided by the CC inequality may be too wide, leading to unsatisfactory results when a higher level of accuracy is needed. In this paper, the chance constraints are reformulated through the so-called Fourth-Moment Method (FMM) for reliability [18]. Unlike the reformulation based on the CC inequality, the FMM does not exhibit the unacceptable outcomes that are observed when a higher precision is required for the risk level associated to the given chance constraints. Specifically, the superior performance of the proposed approach is demonstrated via the optimal control of two different mathematical models of the COVID-19 transmission.

This paper is organized as follows. The mathematical statement of the general CCSOCP is presented in Section 2. The PCE-based technique used to model the propagation of the uncertainties induced by the random parameters through the CCSOCP is described in Section 3. The spectral approach to the efficient computation of the statistical moments of the optimal state variables is outlined in Section 4. Two different approaches to the reformulation of chance constraints are introduced in Section 5. The practical application of the proposed methodology is illustrated in Section 6 via the optimal control of two stochastic mathematical models of the COVID-19 transmission. Finally, the conclusions are reported in Section 7.

2. Chance-constrained stochastic optimal control

2.1. Statement of the chance-constrained stochastic optimal control problem

Consider a probability space $(\Omega, \mathcal{F}, \mathcal{P})$, with Ω being the space of events, $\mathcal{F}$ a σ-algebra, and $\mathcal{P}$ a probability measure. The CCSOCP is stated as follows

$$\min_{\mathbf{u}(t)} \quad \mu_S\left(J(\mathbf{z}(t,\boldsymbol{\zeta}),\mathbf{u}(t),\boldsymbol{\zeta})\right) + \kappa_0 \cdot \sigma_S\left(J(\mathbf{z}(t,\boldsymbol{\zeta}),\mathbf{u}(t),\boldsymbol{\zeta})\right), \tag{1a}$$

subject to:

$$\dot{\mathbf{z}}(t,\boldsymbol{\zeta}) = \mathbf{f}(\mathbf{z}(t,\boldsymbol{\zeta}),\mathbf{u}(t),\boldsymbol{\zeta}) \quad \text{a.s.}, \tag{1b}$$

$$P\left(\mathbf{a}\,\mathbf{z}(t,\boldsymbol{\zeta}) \le \mathbf{b}\right) \ge \mathbf{1} - \boldsymbol{\eta}, \tag{1c}$$

$$\mu_S\left(\mathbf{z}(t_I,\boldsymbol{\zeta})\right) = \mathbf{z}_I, \sigma_S\left(\mathbf{z}(t_I,\boldsymbol{\zeta})\right) \le \varepsilon_I,$$

$$\mu_S\left(\mathbf{z}(t_F,\boldsymbol{\zeta})\right) = \mathbf{z}_F, \sigma_S\left(\mathbf{z}(t_F,\boldsymbol{\zeta})\right) \le \varepsilon_F, \tag{1d}$$

where t denotes time, $\mathbf{z}(t,\boldsymbol{\zeta}) = (z_1(t,\boldsymbol{\zeta}),\dots,z_n(t,\boldsymbol{\zeta}))$ is the vector of stochastic state variables, $\mathbf{u}(t) = (u_1(t),\dots,u_m(t))$ is the vector of control variables, κ_0, ε_I, and ε_F are scalar parameters, $\mathbf{a} = (a_1,\dots,a_{n_C})$, $\mathbf{b} = (b_1,\dots,b_{n_C})$, and $\boldsymbol{\eta} = (\eta_1,\dots,\eta_{n_C})$, with $1 \le n_C \le n$, are vector parameters, and $\boldsymbol{\zeta} = (\zeta_1,\dots,\zeta_{N_U}) \in \Omega$ is the vector of random parameters, whose components are supposed to be independent random variables,. Therefore, the joint PDF of $\boldsymbol{\zeta}$ can be computed as $g(\boldsymbol{\zeta}) = \prod_{i=1}^{N_U} g_i(\zeta_i)$, where $g_i(\zeta_i)$ denotes the marginal PDF of component ζ_i, $i = 1,\dots,N_U$. The initial and final time instants are represented by t_I and t_F, respectively. Vectors $\mathbf{z}_I$ and $\mathbf{z}_F$ denote the initial and final states, respectively. The operators $P(\cdot)$, $\mu_S(\cdot)$, and $\sigma_S(\cdot)$ denote the probability, the expected value, and the standard deviation, respectively.

The objective functional $J(\cdot)$ in (1a) is assumed to be given in Bolza form. Thus, it is formulated as a combination of a Mayer term and a Lagrange term, namely:

$$J(\mathbf{z}(t,\boldsymbol{\zeta}),\mathbf{u}(t),\boldsymbol{\zeta}) = M(\mathbf{z}(t_F,\boldsymbol{\zeta})) + \int_{t_I}^{t_F} L(\mathbf{z}(t,\boldsymbol{\zeta}),\mathbf{u}(t),\boldsymbol{\zeta})\,dt. \tag{2}$$

In (2), the Mayer term, $M(\cdot)$, denotes a terminal cost and the Lagrange term, $L(\cdot)$, denotes a running cost. However, the Lagrange term can be rewritten in Mayer form. Thus, without loss of generality, the objective functional (2) can be assumed to be given in Mayer form [19].

The set of differential Eqs. (1b) represents the dynamical equations of the stochastic epidemic model, whereas the boundary conditions (1d) express the initial and final conditions.

The inequality (1c) represents a chance constraint on the vector of stochastic state variables, with $\mathbf{1} - \boldsymbol{\eta} = (1-\eta_1,\dots,1-\eta_{n_C})$. The term $1-\eta_l$, $l = 1,\dots,n_C$, is usually referred to as guaranteed constraint satisfaction probability or chance constraint probability, whereas the parameter $\eta_l, l = 1,\dots,n_C$, is known as probability of violation or risk level. The formulation of the chance constraint (1c) is understood element-wise, namely

$$P\left(a_1\ z_1(t,\boldsymbol{\zeta}) \le b_1\right) \ge 1-\eta_1,\dots,P\left(a_{n_C}\ z_{n_C}(t,\boldsymbol{\zeta}) \le b_{n_C}\right) \ge 1-\eta_{n_C}, \tag{3}$$

with $1 \le n_C \le n$, meaning that at least a chance constraint is set on one of the components of $\mathbf{z}(t,\boldsymbol{\zeta})$.

Notice that the state variables $\mathbf{z}(t,\boldsymbol{\zeta})$ are functions of both the time t and the random vector $\boldsymbol{\zeta}$. Therefore, the objective functional and the differential equations introduced in (1) are stochastic functions, and the stochastic relations are supposed to be fulfilled almost surely (a.s.). On the contrary, the control variables $\mathbf{u}(t)$ are assumed to be deterministic functions of time t. Moreover, a robust formulation of the objective functional and the boundary conditions is assumed. In particular, the objective functional (1a) is formulated as a weighted sum of the expected value and the standard deviation of the stochastic objective functional (2), being κ_0 the weighting parameter. The robust boundary conditions (1d) are modeled by separating the conditions on the expected value and the standard deviation of the initial and final state values. The expected values of the boundary conditions are assumed to take some specific nominal values, whereas the values of the standard deviation are assumed to fulfill some particular upper bound constraints represented by ε_I and ε_F. The weighting parameter κ_0, the probabilities $\eta_l, l = 1,\dots,n_C$, and the bounds ε_I and ε_F are determined by the designers of the CCSOCP.

2.2. Joint chance constraints

In the statement of the CCSOCP (1), joint chance constraints of the form

$$P\left(a_1\ z_1(t,\boldsymbol{\zeta}) \le b_1,\dots,a_{n_C}\ z_{n_C}(t,\boldsymbol{\zeta}) \le b_{n_C}\right) \ge 1-\eta_J, \quad \text{with} \quad 1 \le n_C \le n, \tag{4}$$

can also be included, since they can be separated into multiple constraints of the form (3) by means of the Bonferroni's inequality [20]. More specifically, the joint chance constraint (4) can be reformulated as

$$P\left(a_1\ z_1(t,\boldsymbol{\zeta}) \ge b_1\right) \le \eta_1,\dots,P\left(a_{n_C}\ z_{n_C}(t,\boldsymbol{\zeta}) \ge b_{n_C}\right) \le \eta_{n_C},$$

with

$$\sum_{l=1}^{n_C} \eta_l = \eta_J.$$

3. Moment-based arbitrary polynomial chaos expansion

Following the spectral technique described in [21], the propagation of the uncertainties induced by the random parameters $\boldsymbol{\zeta} = (\zeta_1, \dots, \zeta_{N_U})$ in the CCSOCP stated in (1) can be represented by means of multi-dimensional polynomial expansions, which are surrogate models of the components of the vector of stochastic state variables $\mathbf{z}(t, \boldsymbol{\zeta})$.

In particular, each state variable $z_l(t, \boldsymbol{\zeta}), l = 1, \dots, n$, is approximated by means of a linear combination of N_P stochastic multivariate orthonormal polynomials $\boldsymbol{\Psi}^l_k(\boldsymbol{\zeta})$ with deterministic coefficients $c^l_k(t)$, namely

$$z_l(t, \boldsymbol{\zeta}) = z_l(t; \zeta_1, \dots, \zeta_{N_U}) \approx \sum_{k=1}^{N_P} c^l_k(t) \cdot \boldsymbol{\Psi}^l_k(\zeta_1, \dots, \zeta_{N_U}),\ l = 1, \dots, n, \tag{5}$$

where the coefficients $c^l_k(t)$, $k = 1, \dots, N_P$, $l = 1, \dots, n$, can be calculated as

$$c^l_k(t) = \int_{\zeta \in \Omega} z_l(t, \boldsymbol{\zeta}) \boldsymbol{\Psi}^l_k(\boldsymbol{\zeta}) d\mathcal{P}(\boldsymbol{\zeta}). \tag{6}$$

To solve the integral (6), different methods can be employed, such as numerical integration, Galerkin projection, or collocation [22]. In this paper, following [23], a Gaussian cubature rule based on the statistical moments of the random vector $\boldsymbol{\zeta} = (\zeta_1, \dots, \zeta_{N_U})$ is used. It is computed in terms of the nodes and weights associated to the multivariate orthonormal polynomials $\boldsymbol{\Psi}^l_k(\boldsymbol{\zeta})$, which are denoted as ζ^{i_j} and $\omega_{i_j}, i = 1, \dots, p, j = 1, \dots, N_U$, respectively, being p the order of the polynomial expansion. The reader is referred to Appendix A for more details.

4. Uncertainty quantification

The statistical moments of the stochastic vector of state variables $\mathbf{z}(t, \boldsymbol{\zeta})$ of the CCSOCP (1) can be efficiently computed through the surrogate models represented by the polynomial expansions (5) [23].

In particular, the first four moments of the stochastic state variables $z_l(t, \boldsymbol{\zeta})$, $l = 1, \dots, n$, can be obtained in terms of scalar products of vectors, which involve the Gaussian cubature nodes and weights introduced in Section 3. More specifically, the mean value, the variance, the skewness, and the kurtosis of $z_l(t, \boldsymbol{\zeta})$, $l = 1, \dots, n$, can be computed, respectively, as

$$\mu_{z_l}(t) = z_l\left(t; \zeta^{i_1}, \dots, \zeta^{i_{N_U}}\right) \cdot \boldsymbol{\omega}, \tag{7a}$$

$$\sigma^2_{z_l}(t) = \left(z_l\left(t; \zeta^{i_1}, \dots, \zeta^{i_{N_U}}\right) - \mu_{z_l}(t)\right)^2 \cdot \boldsymbol{\omega}, \tag{7b}$$

$$\alpha_{3z_l}(t) = \frac{1}{\sigma^3_{z_l}(t)}\left(z_l\left(t; \zeta^{i_1}, \dots, \zeta^{i_{N_U}}\right) - \mu_{z_l}(t)\right)^3 \cdot \boldsymbol{\omega}, \tag{7c}$$

$$\alpha_{4z_l}(t) = \frac{1}{\sigma^4_{z_l}(t)}\left(z_l\left(t; \zeta^{i_1}, \dots, \zeta^{i_{N_U}}\right) - \mu_{z_l}(t)\right)^4 \cdot \boldsymbol{\omega}, \tag{7d}$$

where $\boldsymbol{\omega} = \left(\omega_{i_1}, \dots, \omega_{i_{N_U}}\right)$ is the vector of Gaussian cubature weights, with $i = 1, \dots, p$.

As it will be explained in Section 5, the CCSOCP (1) can be rewritten in terms of the moments (7) of the stochastic state variables $z_l(t, \boldsymbol{\zeta})$, $l = 1, \dots, n$, which in turn are derived from the nodes and weights related to the statistical moments of the input random variables $\boldsymbol{\zeta} = (\zeta_1, \dots, \zeta_{N_U})$.

Moreover, a global sensitivity analysis can be undertaken by computing the so-called Sobol' indices, which provide a comprehensive understanding of the system's sensitivity to the random parameters, based on the variance of the optimal state variables $\mathbf{z}(t, \boldsymbol{\zeta})$. These indices can also be efficiently determined using the coefficients from the expansion (5), as explained in [24]. The reader is referred to Appendix B for more details.

Notice that certain epidemic models consider values such as transmission or recovery rates as time-dependent quantities. Therefore, the uncertainty in the corresponding CCSOCP (1) would be induced by random processes $\zeta_i(t)$, $i = 1, \dots, N_U$, instead of random variables ζ_i, $i = 1, \dots, N_U$. In this case, as explained in [22], the proposed methodology could still be applied. Specifically, each random process ζ_i could be expressed as a linear combination of time-dependent deterministic functions and uncorrelated random variables by means of the so-called Karhunen–Loève (KL) expansion. Then, the spectral approach described in Section 3 would be applied, assuming these uncorrelated random variables provided by the KL expansion as the input random variables of the CCSOCP.

5. Reformulation of the chance constraints

In this section, two different approaches to the reformulation of the chance constraints (3) are presented. The first approach is based on the CC inequality, whereas the second approach relies on the FMM for reliability.

5.1. The Chebyshev-Cantelli's inequality

The chance constraints (3) can be expressed by means of the risk levels η_l and the first two statistical moments of the stochastic state variables $z_l(t, \boldsymbol{\zeta})$, $l = 1, \dots, n_C$. In particular, according to the CC inequality [25], the chance constraint (1c) is equivalent to the deterministic constraint

$$\mathbf{a}^2\ \boldsymbol{\mu}_{\mathbf{z}}(t) + \boldsymbol{\kappa}_{\boldsymbol{\eta}}\ \mathbf{a}\ \boldsymbol{\sigma}_{\mathbf{z}}(t) \leq \mathbf{b}, \tag{8}$$

where $\boldsymbol{\mu}_{\mathbf{z}}(t) = (\mu_{z_1}(t), \dots, \mu_{z_{n_C}}(t))$, $\boldsymbol{\sigma}_{\mathbf{z}}(t) = (\sigma_{z_1}(t), \dots, \sigma_{z_{n_C}}(t))$, and $\boldsymbol{\kappa}_{\boldsymbol{\eta}} = (\kappa_{\eta_1}, \dots, \kappa_{\eta_{n_C}})$, with $\kappa_{\eta_l} = \sqrt{(1-\eta_l)/\eta_l}$, $l = 1, \dots, n_C$. The parameter κ_{η_l} is usually known as the safety parameter [26].

This approach to the reformulation of the chance constraints (3) will be referred to as CC reformulation. Notice that it has been already applied to the chance-constrained stochastic optimal control of epidemic models in [17].

5.2. The fourth-moment method for reliability

The chance constraints (3) are particular cases of constraints of the form

$$P\left(G(z(t, \boldsymbol{\zeta})) \leq 0\right) \geq 1 - \eta_G, \tag{9}$$

which can be expressed in terms of the risk level η_G and the first four moments of the state variable $z(t, \boldsymbol{\zeta})$. More specifically, the probability in the left side of the chance constraint (9), which is referred to as failure probability, can be obtained through the Cumulative Distribution Function (CDF) of a standard Gaussian random variable using the Higher-Order Moments Standardization Technique (HOMST) [18].

In particular, the failure probability for the performance function $G(z(t, \boldsymbol{\zeta}))$ based on the FMM for reliability can be computed as

$$P\left(G(z(t, \boldsymbol{\zeta})) \leq 0\right) = \Phi(-\beta_{FM}(t)), \tag{10}$$

where $\Phi(\cdot)$ denotes the CDF of a standard normal random variable, and

$$\beta_{FM}(t) = \frac{3(\alpha_{4G}(t) - 1)\beta_{SM}(t) + \alpha_{3G}(t)(\beta^2_{SM}(t) - 1)}{\sqrt{(9\alpha_{4G}(t) - 5\alpha^2_{2G}(t) - 9)(\alpha_{4G}(t) - 1)}} \tag{11}$$

with

$$\beta_{SM}(t) = \frac{\mu_G(t)}{\sigma_G(t)}, \tag{12}$$

being $\mu_G(t)$, $\sigma_G(t)$, $\alpha_{3G}(t)$, and $\alpha_{4G}(t)$ the mean value, the standard deviation, the skewness, and the kurtosis of $G(z(t, \boldsymbol{\zeta}))$, respectively. Notice that $\beta_{SM}(t)$ and $\beta_{FM}(t)$ are referred to as the reliability indexes based on the second-moment and the fourth-moment method, respectively. Alternatively, as shown in [18], the failure probability for the performance function $G(z(t, \boldsymbol{\zeta}))$ derived from the HOMST can be obtained using the Edgeworth expansion [27]. The reader is referred to Appendix C for more details.

This approach to the reformulation of the chance constraints (3) will be referred to as FMM reformulation.

5.3. Reformulation of the chance-constrained stochastic optimal control problem

The surrogate models of the state variables $z_l(t,\boldsymbol{\zeta})$, $l=1,\dots,n$, provided by the polynomial expansions (5), allow the numerical resolution of the CCSOCP formulated in (1) to be carried out. In particular, the objective functional (1a), the stochastic differential Eqs. (1b), the chance constraint (1c), and the boundary conditions (1d) can be reformulated by means of the computational and statistical properties of the polynomial expansions described in Section 4, together with the two reformulation approaches described in Sections 5.1 and 5.2.

Specifically, the CCSOCP defined in (1) can be rewritten as the following deterministic Optimal Control Problem (OCP)

$$\min_{\mathbf{u}(t)} \quad \mu_M(t_F)+\kappa_0\cdot\sigma_M(t_F), \tag{13a}$$

subject to:

$$\dot{\mathbf{z}}_1(t,\boldsymbol{\zeta}_1)=\mathbf{f}(\mathbf{z}(t,\boldsymbol{\zeta}_1),\mathbf{u}(t),\boldsymbol{\zeta}_1), \tag{13b}$$

$$\dot{\mathbf{z}}_2(t,\boldsymbol{\zeta}_2)=\mathbf{f}(\mathbf{z}(t,\boldsymbol{\zeta}_2),\mathbf{u}(t),\boldsymbol{\zeta}_2), \tag{13c}$$

...

$$\dot{\mathbf{z}}_p(t,\boldsymbol{\zeta}_p)=\mathbf{f}(\mathbf{z}(t,\boldsymbol{\zeta}_p),\mathbf{u}(t),\boldsymbol{\zeta}_p), \tag{13d}$$

$$\mathbf{a}^2\ \boldsymbol{\mu}_{\mathbf{z}}(t)+\boldsymbol{\kappa}_{\boldsymbol{\eta}}\ \mathbf{a}\ \boldsymbol{\sigma}_{\mathbf{z}}(t)\le\mathbf{b} \quad \text{or} \quad \boldsymbol{\Phi}(-\boldsymbol{\beta}_{FM}(t))\le\mathbf{1}-\boldsymbol{\eta}. \tag{13e}$$

$$\boldsymbol{\mu}_{\mathbf{z}}(t_I)=\mathbf{z}_I,\ \boldsymbol{\sigma}_{\mathbf{z}}(t_I)\le\boldsymbol{\varepsilon}_I,\ \boldsymbol{\mu}_{\mathbf{z}}(t_F)=\mathbf{z}_F,\ \boldsymbol{\sigma}_{\mathbf{z}}(t_F)\le\boldsymbol{\varepsilon}_F, \tag{13f}$$

where $\boldsymbol{\Phi}(-\boldsymbol{\beta}_{FM}(t)) = \left(\Phi(-\beta_{FM_1}(t)),\dots,\Phi(-\beta_{FM_{n_C}}(t))\right)$, with $\Phi(-\beta_{FM_l}(t))$ being the failure probability associated to the state variable $z_l(t,\boldsymbol{\zeta})$, $l=1,\dots,n_C$.

According to (13a), the objective functional (1a) is expressed in terms of $\mu_M(t)$ and $\sigma_M(t)$, which are calculated using (7a) and (7b) and denote, respectively, the mean value and the standard deviation of the state variable $z_M(t,\boldsymbol{\zeta})$ introduced to reformulate the objective functional (2) in Mayer form.

The reformulation of the stochastic differential equations consist of the set of deterministic differential Eqs. (13b)–(13d), which is obtained by substituting the random parameter vector $\boldsymbol{\zeta}=(\zeta_1,\dots,\zeta_{N_U})$ in (1b) with the multivariate nodes $\boldsymbol{\zeta}_i=(\zeta^{i_1},\dots,\zeta^{i_{N_U}})$, $i=1,\dots,p$.

Based on (13e), either one of the two approaches described in Sections 5.1 and 5.2, can be used to rewrite the chance constraints (1c). Thus, if the CC inequality is employed, the chance constraints will be reformulated using the first two moments of the state variables $z_l(t,\boldsymbol{\zeta})$, $l=1,\dots,n_C$, whereas, if the FMM is used, they will be expressed in terms of the first four moments, which are calculated using (7).

Finally, according to (13f), the boundary conditions (1d), can be written in terms of the expected value and standard deviation of the state variables using (7a) and (7b).

Since (13) is a deterministic OCP, it can be solved using any conventional numerical method devised for solving continuous OCPs. Specifically, the Hermite-Simpson direct collocation technique is used in this paper [28].

The flow chart represented in Fig. 1 summarizes the computational steps required to solve the CCSOCP (1) using the proposed approach.

6. Chance-constrained stochastic optimal control of the COVID-19 transmission

In this section, various numerical experiments are conducted using two different stochastic mathematical models of the COVID-19 transmission. First, the CC and FMM reformulations are compared through the chance-constrained optimal control of the so-called SEIsIaQRS model considered in [17]. Then, the capability of the proposed FMM reformulation to deal with larger, more complex epidemic models derived from real-world data is analyzed via the chance-constrained optimal control of the so-called SIDARTHE model introduced in [29].

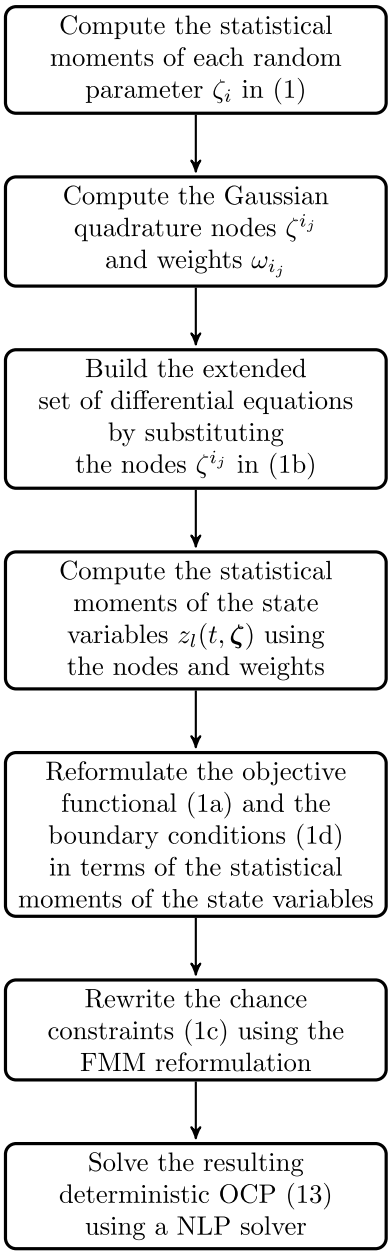

Fig. 1. Computational steps for the resolution of the CCSOCP stated in (1).

6.1. SEIsIaQRS model

As mentioned in Section 5.1, the CC reformulation has already been applied to the chance-constrained stochastic optimal control of epidemic models in [17]. Moreover, the accuracy of the corresponding spectral surrogate of the SEIsIaQRS epidemic model has been already assessed in [30]. Therefore, for the sake of comparison, the same stochastic optimal control problem stated in [17] has been considered in this work, in which the underlying dynamical system consists of a COVID-19 epidemic model with 6 compartments, namely susceptible (S), exposed (E), symptomatic (I_s), asymptomatic (I_a), isolated (Q), and recovered (R) subjects. The flow chart of this epidemic model is represented in Fig. 2. More specifically, the stochastic optimal control problem is formulated as follows

$$\min_{\upsilon(t),\kappa_a(t)} \quad M_J(t,\boldsymbol{\zeta})+\kappa_0\cdot\Sigma_J(t,\boldsymbol{\zeta}) \tag{14a}$$

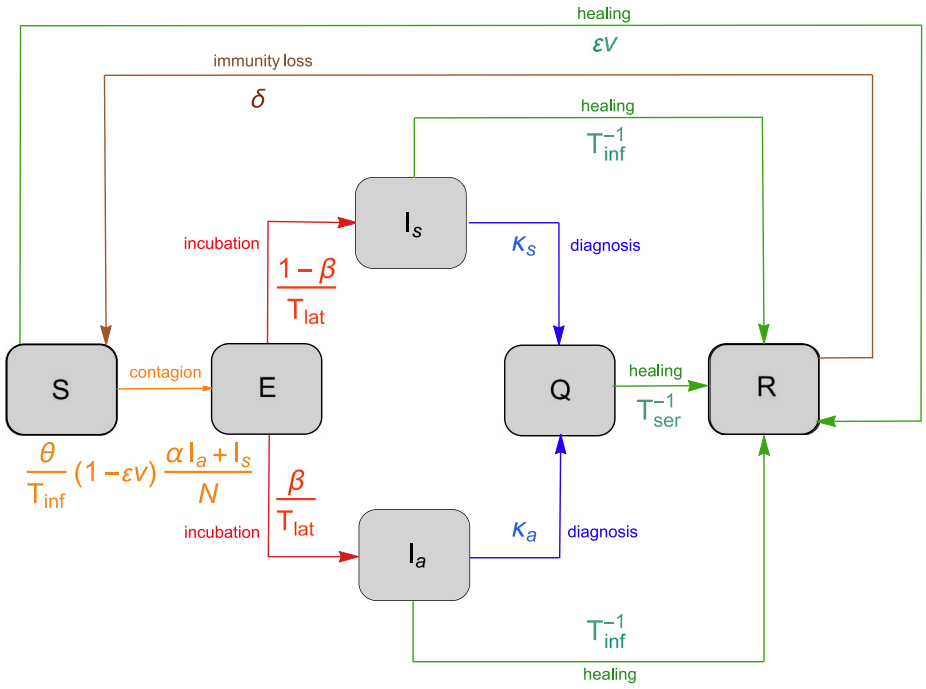

Fig. 2. Flow chart of the SEIsIaQRS epidemic model (14b)–(14g).

subject to:

$$\dot{S}(t,\zeta) = -\frac{\theta}{T_{inf}}(1-\varepsilon v(t))\frac{I(t,\zeta)}{N}S(t,\zeta) - \varepsilon v(t)S(t,\zeta) + \delta R(t,\zeta) \text{ a.s.,} \quad (14b)$$

$$\dot{E}(t,\zeta) = \frac{\theta}{T_{inf}}(1-\varepsilon v(t))\frac{I(t,\zeta)}{N}S(t,\zeta) - \frac{E(t,\zeta)}{T_{lat}} \text{ a.s.,} \quad (14c)$$

$$\dot{I}_s(t,\zeta) = (1-\beta)\frac{E(t,\zeta)}{T_{lat}} - \left(\kappa_s + \frac{1}{T_{inf}}\right) I_s(t,\zeta) \text{ a.s.,} \quad (14d)$$

$$\dot{I}_a(t,\zeta) = \beta\frac{E(t,\zeta)}{T_{lat}} - \left(\kappa_a(t) + \frac{1}{T_{inf}}\right) I_a(t,\zeta) \text{ a.s.,} \quad (14e)$$

$$\dot{Q}(t,\zeta) = \kappa_s I_s(t,\zeta) + \kappa_a(t) I_a(t,\zeta) - \frac{Q(t,\zeta)}{T_{ser}} \text{ a.s.,} \quad (14f)$$

$$\dot{R}(t,\zeta) = \frac{I_s(t,\zeta) + I_a(t,\zeta)}{T_{inf}} + \frac{Q(t,\zeta)}{T_{ser}} + \varepsilon v(t)S(t,\zeta) - \delta R(t,\zeta) \text{ a.s.,} \quad (14g)$$

$$\mu_S\left(S(t_I,\zeta)\right) = S_I, \quad \mu_S\left(E(t_I,\zeta)\right) = E_I, \quad \mu_S\left(I_s(t_I,\zeta)\right) = I_{s_I}, \quad (14h)$$

$$\mu_S\left(I_a(t_I,\zeta)\right) = I_{a_I}, \quad \mu_S\left(Q(t_I,\zeta)\right) = Q_I, \quad \mu_S\left(R(t_I,\zeta)\right) = R_I, \quad (14i)$$

$$\sigma_S\left(S(t_I,\zeta)\right) \le \varepsilon_I, \quad \sigma_S\left(E(t_I,\zeta)\right) \le \varepsilon_I, \quad \sigma_S\left(I_s(t_I,\zeta)\right) \le \varepsilon_I, \quad (14j)$$

$$\sigma_S\left(I_a(t_I,\zeta)\right) \le \varepsilon_I, \quad \sigma_S\left(Q(t_I,\zeta)\right) \le \varepsilon_I, \quad \sigma_S\left(R(t_I,\zeta)\right) \le \varepsilon_I, \quad (14k)$$

where $I(t,\zeta) = I_s(t,\zeta) + \alpha_I I_a(t,\zeta)$, $\zeta = (\theta, \varepsilon, \delta)$ is the vector of random parameters, and $v(t) \in [0, v_U]$ and $\kappa_a(t) \in [0, \kappa_U]$ denote the deterministic control variables that represent the vaccination and testing rates, respectively, with v_U and κ_U being upper bounds, which are determined by the designers of the stochastic optimal control problem according to their preferences. The value and meaning of the parameters in (14) are described in Table 1. The reader is referred to [17] for further details.

In the objective functional (14a), $M_J(t,\zeta) = \mu_S\left(J(I_s(t,\zeta), I_a(t,\zeta), v(t), \kappa_a(t), \zeta)\right)$, and $\Sigma_J(t,\zeta) = \sigma_S\left(J(I_s(t,\zeta), I_a(t,\zeta), v(t), \kappa_a(t), \zeta)\right)$, where

$$J(I_s(t,\zeta), I_a(t,\zeta), v(t), \kappa_a(t), \zeta) = \int_{t_I}^{t_F} \left(C_1 \cdot I_s(t,\zeta) + C_2 \cdot I_a(t,\zeta) + C_3 \cdot v^2(t) + C_4 \cdot \kappa_a^2(t)\right) dt, \quad (15)$$

with $C_i, i = 1,2,3,4$, being weights, which are specified by the designers of the stochastic optimal control problem according to their preferences.

Table 1
Value and meaning of the model parameters used in the numerical experiments A and B [17].

Parameter	Meaning	Value	Units
α	Asymptomatic over symptomatic subjects ratio	1.000	Dimensionless
β	Population ratio that remains asymptomatic	0.800	Dimensionless
δ	Immunity loss	Random	$Days^{-1}$
ε	Vaccine efficacy	Random	Dimensionless
κ_s	Isolation rate of symptomatic subjects	0.950	Dimensionless
θ	Replication factor	Random	Dimensionless
T_{ser}	Mean serial time interval	7.500	Days
T_{lat}	Mean incubation period	5.200	Days
T_{inf}	Mean infectious period	2.300	Days

Following [17], a non-dimensionalized form of the stochastic optimal control problem (14) has been used in all the experiments presented in this section, along with the initial conditions:
$(S_0 = 0.84908, E_0 = 0.00102, I_{s_0} = 0.0002, I_{a_0} = 0.0008,$
$Q_0 = 0, R_0 = 0.1489)$.
Moreover, the replication factor θ has been assumed to follow a gamma distribution G(3500, 0.001), the vaccine efficacy ε a beta distribution B(160, 10), and the immunity loss rate δ a beta distribution B(20, 6000). Furthermore, the order of the aPC expansion has been set to $p = 4$, the upper bounds have been set to $\varepsilon_I = 10^{-6}$, $v_U = 0.007$, and $\kappa_U = 0.5$, and the weighting parameters have been set to $\alpha_I = 1$, $C_1 = 0.15, C_2 = 0.095, C_3 = 0.75$, and $C_4 = 0.005$.

6.1.1. Experiment A

In this experiment, for all $t \in [t_I, t_F]$, the chance constraint

$$P\left(I_a(t,\zeta) \le I_{a_U}\right) \ge 1 - \eta_a \quad (16)$$

has been added to the stochastic optimal control problem (14), and the resulting CCSOCP has been solved using both the CC and the FMM reformulations. Specifically, to mitigate the spread of the disease, the upper bound on the proportion of daily asymptomatic infected subjects

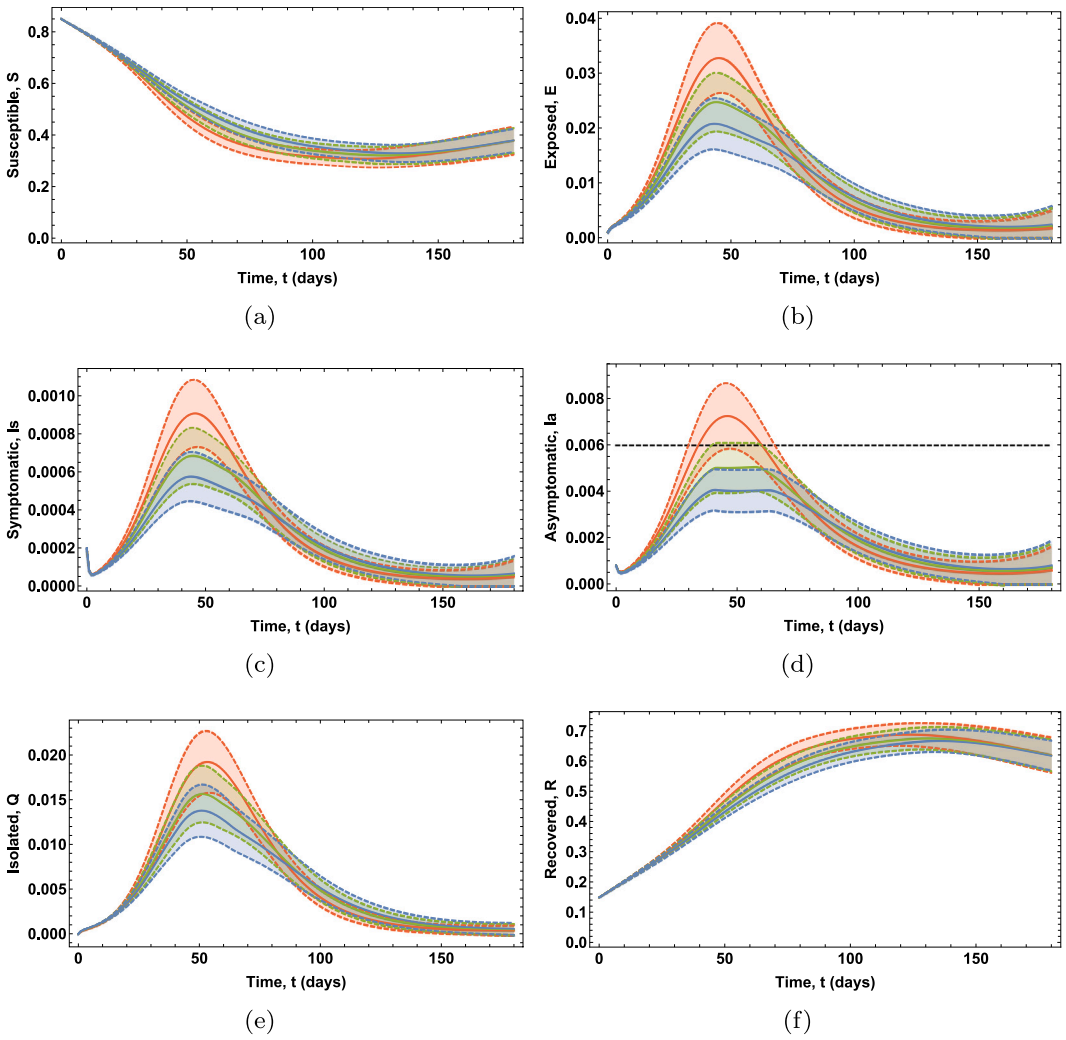

Fig. 3. Experiment A. Expected values of the proportions of subjects for each state variable, along with the corresponding 2-sigma confidence envelope. The optimal solutions obtained using the CC and the FMM reformulations are shown in blue and green, respectively. The optimal solutions obtained without chance constraint are shown in red.

Table 2
Experiment A. Maximum scores of the upper values of the 2-sigma confidence envelopes for the optimal state variables E, I_s, I_a, and Q.

	E	I_s	I_a	Q
WC	0.0391	0.0011	0.0087	0.0226
CC	0.0254	0.0007	0.0013	0.0167
FMM	0.0300	0.0008	0.0061	0.0188

has been set to $I_{a_U} = 0.006$ and the corresponding risk level has been set to $\eta_a = 0.05$.

Fig. 3 shows the expected values of the proportions of subjects for each optimal state variable, along with the corresponding 2-sigma confidence envelopes obtained using both the CC and the FMM reformulations, which are represented in blue and green lines, respectively. The associated deterministic optimal control variables are depicted in Fig. 4. For the sake of comparison, Figs. 3 and 4 also include the optimal solutions of the SOCP (14) represented in red lines, namely the optimal solutions obtained if the chance constraint (16) is not considered. The maximum scores of the upper values of the corresponding 2-sigma confidence envelopes are reported in Table 2 for the state variables E, I_s, I_a, and Q, where WC stands for without constraints.

The influence of the chance constraint (16) on the optimal solutions can be clearly appreciated in Fig. 3, particularly in Fig. 3.d, when compared to the optimal solutions obtained without considering such constraint. The reduction in the proportion of asymptomatic subjects caused by constraint (16) is mainly achieved at the expense of increasing the testing of asymptomatic subjects during the first third of the time interval, as it can be seen in Fig. 4.b.

However, a noticeable difference exists between the solutions provided by the two reformulations. The 2-sigma confidence envelope for the proportion of asymptomatic subjects provided by the CC reformulation complies amply with the chance constraint. In other words, the chance constraint is not binding. Conversely, the envelope corresponding to the FMM reformulation saturates the chance constraint, indicating that the chance constraint is binding in this case.

Monte Carlo (MC) simulations have been conducted using the corresponding aPC surrogate models of the optimal proportion of asymptomatic subjects computed from both the CC and the FMM reformulations. For the sake of clarity, Fig. 5 shows a random selection of 100 runs. According to these MC simulations, the estimated probability of a threshold violation is 0.0546 for the FMM reformulation, whereas it is 0.001 for the CC reformulation. The latter is significantly lower than the predetermined risk level $\eta_a = 0.05$. This undesirable behavior worsens as the risk level decreases.

Fig. 6 shows the optimal proportions of asymptomatic subjects obtained using both the CC and the FMM reformulations for different values of the risk level η_a, ranging from 0.00001 to 0.05. For the sake of clarity, only the upper values of the 2-sigma confidence envelopes are

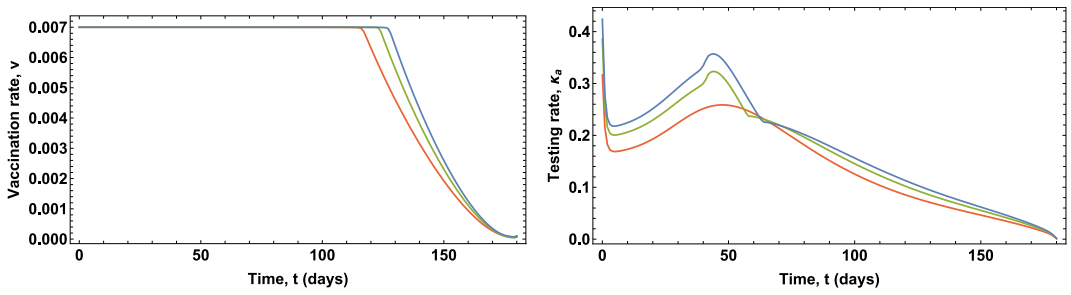

Fig. 4. Experiment A. Optimal vaccination and testing rates. The optimal controls obtained using the CC and the FMM reformulations are shown in blue and green, respectively. The optimal controls obtained without chance constraint are shown in red.

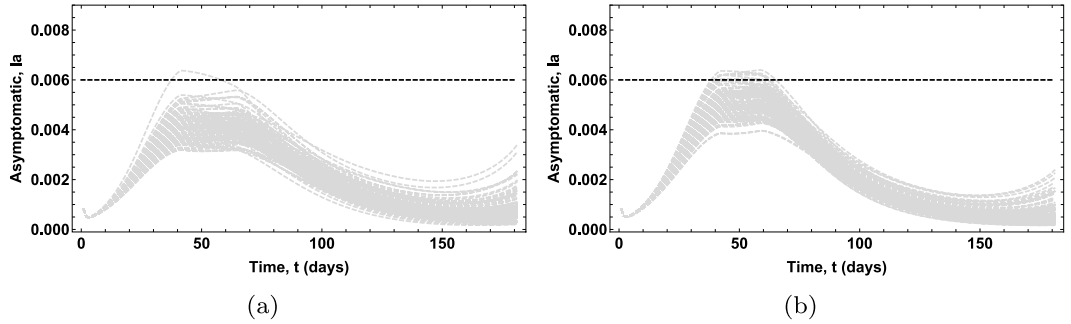

Fig. 5. Experiment A. MC simulations of the proportion of asymptomatic subjects using the CC reformulation (left) and the FMM reformulation (right).

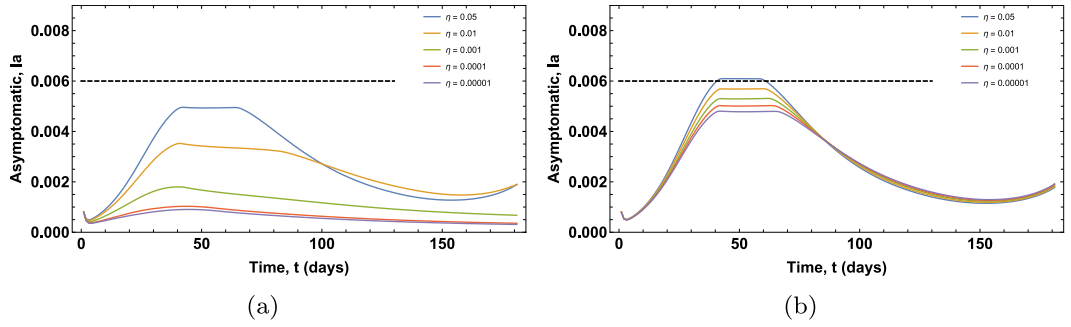

Fig. 6. Experiment A. Proportions of asymptomatic subjects obtained using the CC reformulation (left) and the FMM reformulation (right) for different values of the risk level η_a. For the sake of clarity, only the upper values of the 2-sigma confidence envelopes have been depicted.

depicted. The corresponding optimal vaccination and testing rates are shown in Fig. 7. With the CC reformulation, as the risk level decreases, the curve representing the proportion of asymptomatic subjects flattens excessively, which results in inefficient or even impractical control strategies for the public health system. Conversely, when the FMM reformulation is used, both the proportion of asymptomatic subjects and the associated optimal controls evolve consistently as the risk level varies.

Finally, the Sobol' indices corresponding to the optimal solutions of the CCSOCP obtained using the CC and the FMM reformulations are shown in Fig. 8, which are depicted in dashed and solid lines, respectively. Specifically, the Sobol' indices associated with the random parameters θ, ε, and δ are represented in blue, orange, and green colors, respectively. The Sobol' indices computed from both reformulations show similar trends. In particular, the variance of the state variables E, I_s, I_a, and Q, which can be attributed to the variance of ε is almost insignificant. Besides, the variance of the state variables S and R shows minor yet noteworthy values within the first 30 days. Furthermore, the relative impact of the variance of θ and δ on the variance of the state variables E, I_s, I_a, and Q fluctuates over the considered time span. More specifically, the variance of θ primarily influences the variance of these state variables for the initial 80 days, while the variance of δ takes over as the dominant influence during the subsequent 100 days.

6.1.2. Experiment B

In this experiment, for all $t \in [t_I, t_F]$, the joint chance constraint

$$P\left(I_s(t,\zeta) \le I_{s_U}, I_a(t,\zeta) \le I_{a_U}\right) \ge 1 - \eta_J, \tag{17}$$

with $\eta_J = \eta_s + \eta_a$, has been added to the stochastic optimal control problem (14), and the resulting CCSOCP has been solved using both the CC and the FMM reformulations. Specifically, the upper bounds on the proportion of daily symptomatic and asymptomatic infected subjects have been set to $I_{s_U} = 0.0006$ and $I_{a_U} = 0.006$, respectively, and the corresponding risk levels have been set to $\eta_s = \eta_a = 0.025$.

Fig. 9 shows the optimal proportions of symptomatic and asymptomatic subjects obtained using both the CC and the FMM reformulations for different values of the joint risk level η_J, ranging from 0.00001 to 0.05. In all cases, the risk levels η_s and η_a are assumed to be equal. For the sake of clarity, only the upper values of the 2-sigma confidence envelopes are depicted. The corresponding optimal vaccination and

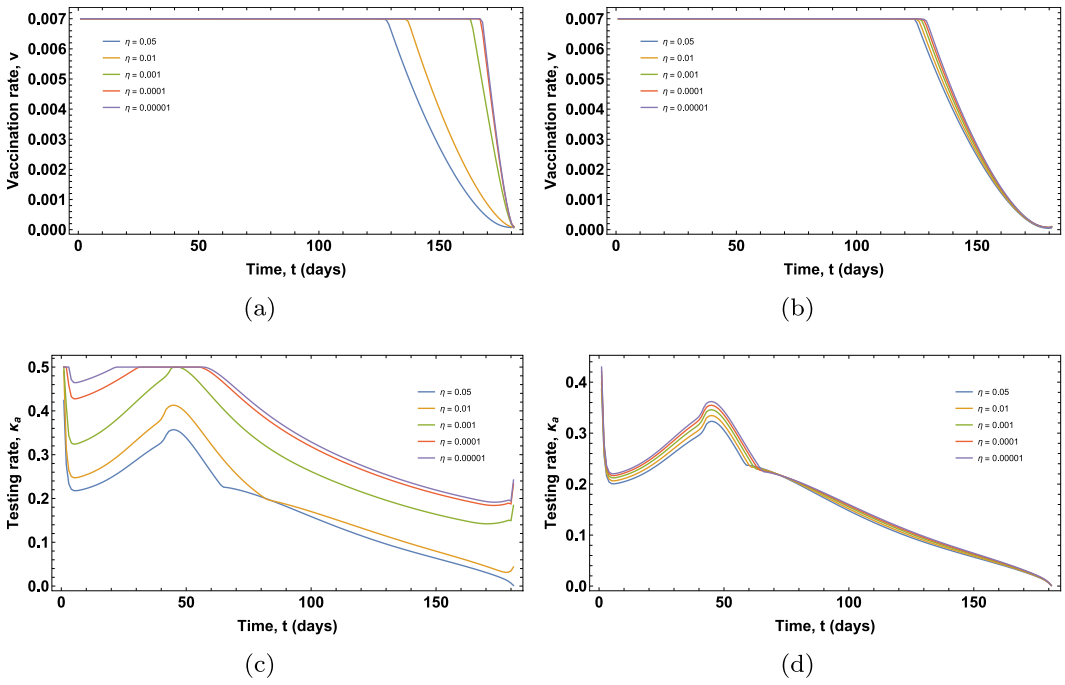

Fig. 7. Experiment A. Optimal vaccination and testing rates obtained using the CC reformulation (left) and the FMM reformulation (right) for different values of the risk level η_a.

Table 3
Nominal value and meaning of the model parameters used in the numerical experiments C and D.

Parameter	Meaning	Nominal value	Unit
α	Susceptible-infected transmission rate	0.570	People per day
β	Susceptible-diagnosed transmission rate	0.011	People per day
γ	Susceptible-ailing transmission rate	0.456	People per day
δ	Susceptible-recognized transmission rate	0.011	People per day
θ	Symptomatic testing rate	0.371	Dimensionless
ζ	Unaware relevant symptoms rate	0.125	$Days^{-1}$
η	Aware relevant symptoms rate	0.125	$Days^{-1}$
μ	Undetected life-threatening symptoms rate	0.017	$Days^{-1}$
ν	Detected life-threatening symptoms rate	0.027	$Days^{-1}$
τ	Mortality rate	0.010	$Days^{-1}$
λ	Infected recovery rate	0.034	$Days^{-1}$
κ	Diagnosed recovery rate	0.017	$Days^{-1}$
ξ	Ailing recovery rate	0.017	$Days^{-1}$
ρ	Recognized recovery rate	0.034	$Days^{-1}$
σ	Threatened recovery rate	0.017	$Days^{-1}$

testing rates are shown in Fig. 10. As in Experiment A, an undesirable outcome is obtained when using the CC reformulation. In contrast, the FMM reformulation provides the expected result. More specifically, in this case, the constraint on the proportion of symptomatic subjects is binding, being the primary cause of the rise in the testing rate, which in turn implies that the constraint on the proportion of asymptomatic subjects is not binding.

6.2. SIDARTHE model

In order to further test the practical applicability of the proposed FMM reformulation, a second epidemic model has been considered as a benchmark. This model, referred to as the SIDARTHE model, has been fitted from real-world data. Both the mathematical model and the data are freely available online [29]. Specifically, the underlying dynamical system consists of a COVID-19 epidemic model with 8 compartments, namely susceptible (S), infected (I), diagnosed (D), ailing (A), recognized (R), threatened (T), healed(H), and extinct (E) subjects. The flow chart of this epidemic model is represented in Fig. 11. In particular, the stochastic optimal control of the SIDARTHE model is formulated as follows

$$\min_{v(t),\,\varepsilon(t)} \quad \mu_S\left(J(I(t,\zeta),\varepsilon(t),\zeta)\right)+\kappa_0\cdot\sigma_S\left(J(I(t,\zeta),\varepsilon(t),\zeta)\right), \tag{18a}$$

subject to:

$$\dot{S}(t,\zeta)=-S(t,\zeta)\Lambda(t,\zeta)\ \text{a.s.}, \tag{18b}$$
$$\dot{I}(t,\zeta)=S(t,\zeta)\ \Lambda(t,\zeta)-(\varepsilon(t)+\zeta+\lambda)I(t,\zeta)\ \text{a.s.}, \tag{18c}$$
$$\dot{D}(t,\zeta)=\varepsilon(t)I(t,\zeta)-(\eta+\rho)D(t,\zeta)\ \text{a.s.}, \tag{18d}$$
$$\dot{A}(t,\zeta)=\zeta I(t,\zeta)-(\theta+\mu+\kappa)A(t,\zeta)\ \text{a.s.}, \tag{18e}$$
$$\dot{R}(t,\zeta)=\eta D(t,\zeta)+\theta A(t,\zeta)-(\nu+\xi)R(t,\zeta)\ \text{a.s.}, \tag{18f}$$
$$\dot{T}(t,\zeta)=\mu A(t,\zeta)+\nu R(t,\zeta)-(\sigma+\tau)T(t,\zeta)\ \text{a.s.}, \tag{18g}$$
$$\dot{H}(t,\zeta)=\lambda I(t,\zeta)+\rho D(t,\zeta)+\kappa A(t,\zeta)+\xi R(t,\zeta)+\sigma T(t,\zeta)\ \text{a.s.}, \tag{18h}$$
$$\dot{E}(t,\zeta)=\tau T(t,\zeta)\ \text{a.s.}, \tag{18i}$$

$$\mu_S\left(S(t_I,\zeta)\right)=S_I,\mu_S\left(I(t_I,\zeta)\right)=I_I,$$

$$\mu_S\left(D(t_I,\zeta)\right)=D_I,\mu_S\left(A(t_I,\zeta)\right)=A_I, \tag{18j}$$

$$\mu_S\left(R(t_I,\zeta)\right)=R_I,\mu_S\left(T(t_I,\zeta)\right)=T_I,$$

$$\mu_S\left(H(t_I,\zeta)\right)=H_I,\mu_S\left(E(t_I,\zeta)\right)=E_I, \tag{18k}$$

$$\sigma_S\left(S(t_I,\zeta)\right)\le\varepsilon_I,\sigma_S\left(I(t_I,\zeta)\right)\le\varepsilon_I,\sigma_S\left(D(t_I,\zeta)\right)\le\varepsilon_I,$$

$$\sigma_S\left(A(t_I,\zeta)\right)\le\varepsilon_I, \tag{18l}$$

$$\sigma_S\left(R(t_I,\zeta)\right)\le\varepsilon_I,\sigma_S\left(T(t_I,\zeta)\right)\le\varepsilon_I,\sigma_S\left(H(t_I,\zeta)\right)\le\varepsilon_I,$$

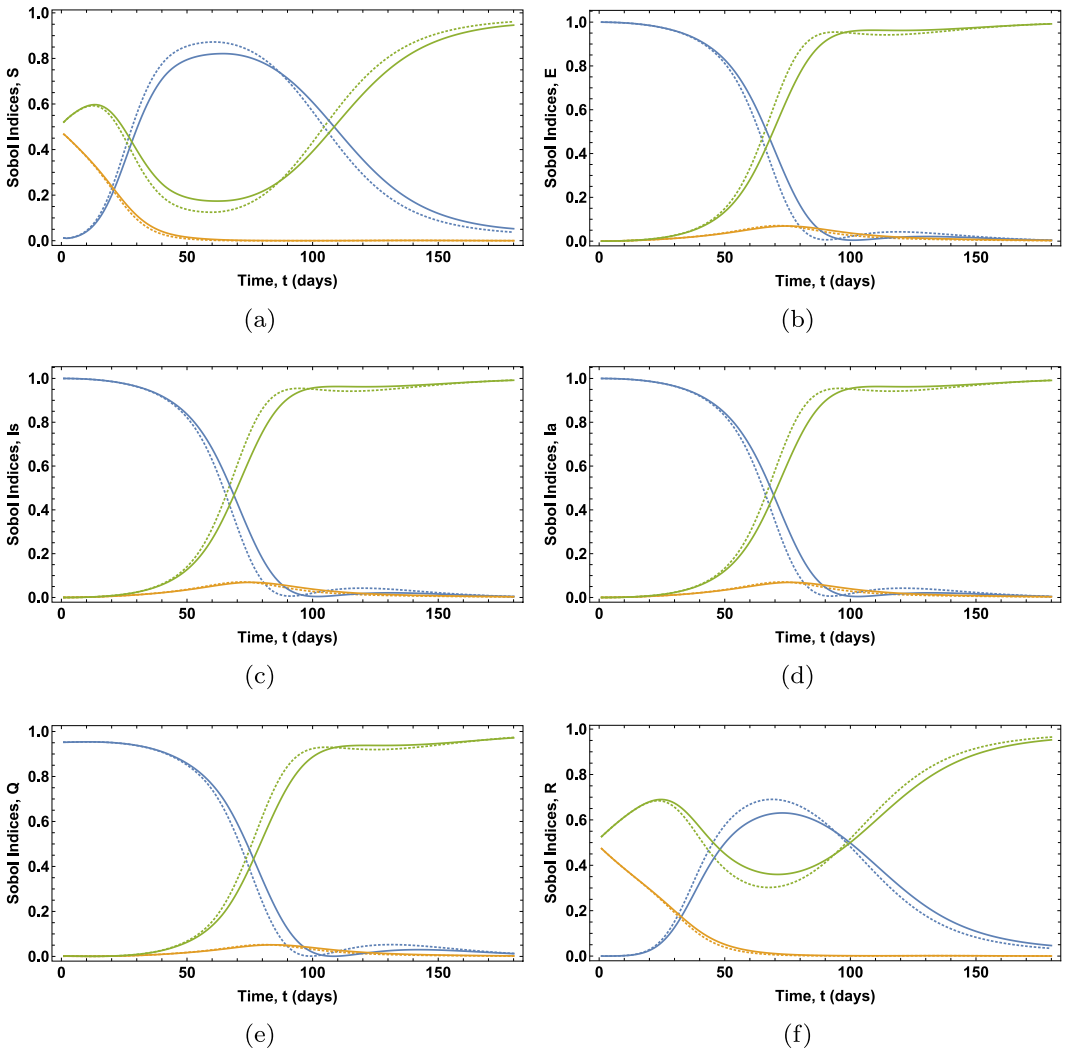

Fig. 8. Experiment A. Sobol' indices associated with θ (blue), ε (orange), and δ (green). The curves obtained in the solution of the CCSOCP with the CC and the FMM reformulation are shown in dashed and solid lines, respectively.

$$\sigma_S\left(E(t_I,\boldsymbol{\zeta})\right) \leq \varepsilon_I, \tag{18m}$$

where $\Lambda(t,\boldsymbol{\zeta}) = \alpha I(t,\boldsymbol{\zeta}) + \beta D(t,\boldsymbol{\zeta}) + \gamma A(t,\boldsymbol{\zeta}) + \delta R(t,\boldsymbol{\zeta})$, $\boldsymbol{\zeta} = (\alpha,\beta,\gamma,\delta,\lambda,\kappa,\xi,\rho,\sigma)$ is the vector of random parameters, and $\varepsilon(t) \in [0,\varepsilon_U]$ denote the deterministic control variable that represents the testing rate for the detection of asymptomatic infected subjects, ε_U being an upper bound, which is determined by the designers of the stochastic optimal control problem according to their preferences. Notice that ε is considered as a constant parameter in [29]. The nominal value and meaning of the parameters in (18) are described in Table 3.

In the objective functional (18a),

$$J(I(t,\boldsymbol{\zeta}),\varepsilon(t),\boldsymbol{\zeta}) = \int_{t_I}^{t_F} \left(C_1 \cdot I(t,\boldsymbol{\zeta}) + C_2 \cdot \varepsilon^2(t)\right) dt,$$

with $C_i, i = 1,2$, being weights, which are specified by the designers of the stochastic optimal control problem according to their preferences.

According to [29], a non-dimensionalized form of the stochastic optimal control problem (18) has been used, along with the initial conditions: $S_0 = 0.999996, I_0 = 3.33 \cdot 10^{-6}, D_0 = 3.33 \cdot 10^{-7}, A_0 = 1.67 \cdot 10^{-8}, R_0 = 3.33 \cdot 10^{-8}, T_0 = 0, H_0 = 0$, and $E_0 = 0$. Moreover, all the components of the vector of random parameters $\boldsymbol{\zeta} = (\alpha,\beta,\gamma,\delta,\lambda,\kappa,\xi,\rho,\sigma)$ have been modeled by adding a 5% Gaussian noise to their corresponding nominal values. In other words, all the transmission and recovery rates of the SIDARTHE model have been assumed to be random parameters. Furthermore, the order of the aPC expansion has been set to $p = 3$, the upper bounds have been set to $\varepsilon_I = 10^{-6}$ and $\varepsilon_U = 0.4$, and the weighting parameters have been set to $C_1 = C_2 = 0.01$.

6.2.1. *Experiment C*

In this experiment, the computational scalability of the proposed method is tested on the stochastic optimal control problem (18). Moreover, a sensitivity analysis is carried out to identify which components of the vector of random parameters $\boldsymbol{\zeta} = (\alpha,\beta,\gamma,\delta,\lambda,\kappa,\xi,\rho,\sigma)$ have more influence on the variability of the optimal stochastic state variables obtained in the solution of (18).

To analyze the scalability of the proposed approach, the number of iterations and CPU time required to solve the stochastic optimal control problem (18) for different sizes N_U of the vector of random parameters $\boldsymbol{\zeta}$ have been calculated. Specifically, a full tensor cubature, with order of the polynomial expansion $p = 4$, has been used for $N_U = 1,2,3$, whereas a Smolyak cubature, with order $p = 4$ and level $\imath = 3$, has been employed for $N_U = 4,5,6,7,8,9$. The obtained mean number of iterations (#iter) and mean CPU time (CPUT) are reported in Table 4, along with the number of weights (#CW) required to perform the corresponding Gaussian cubature. It can be concluded that, despite the availability of the sparse-grid cubature, the computational burden of the stochastic optimal control problem increases significantly as the size of the vector of random parameters grows. Thus, a sensitivity analysis

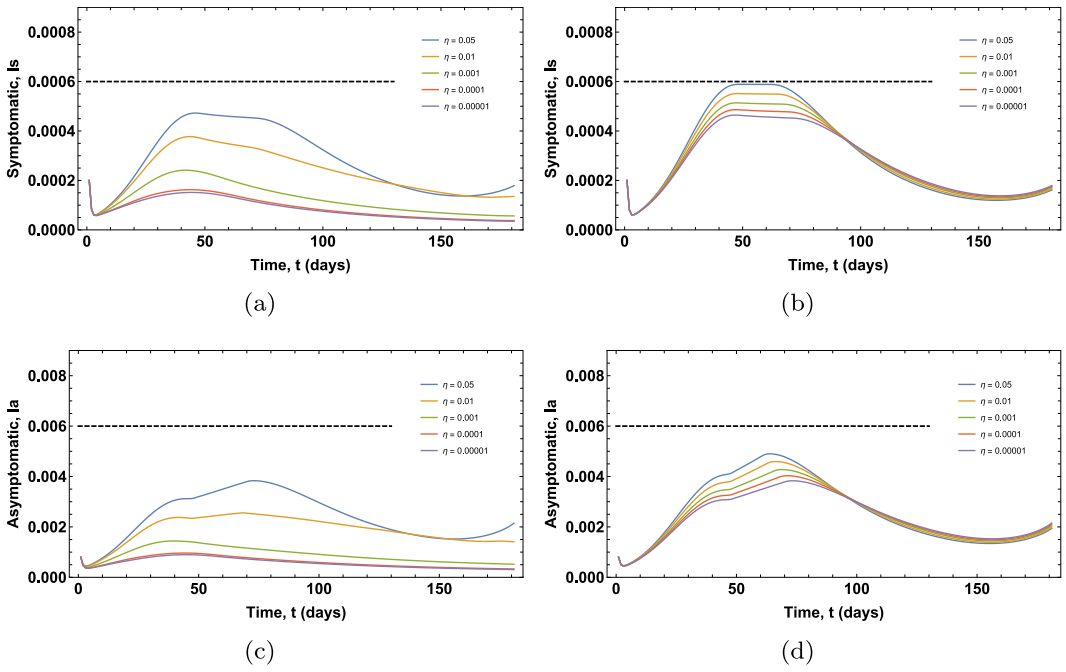

Fig. 9. Experiment B. Proportions of symptomatic and asymptomatic subjects obtained using the CC reformulation (left) and the FMM reformulation (right) for different values of the joint risk level η_J. For the sake of clarity, only the upper values of the 2-sigma confidence envelopes have been depicted.

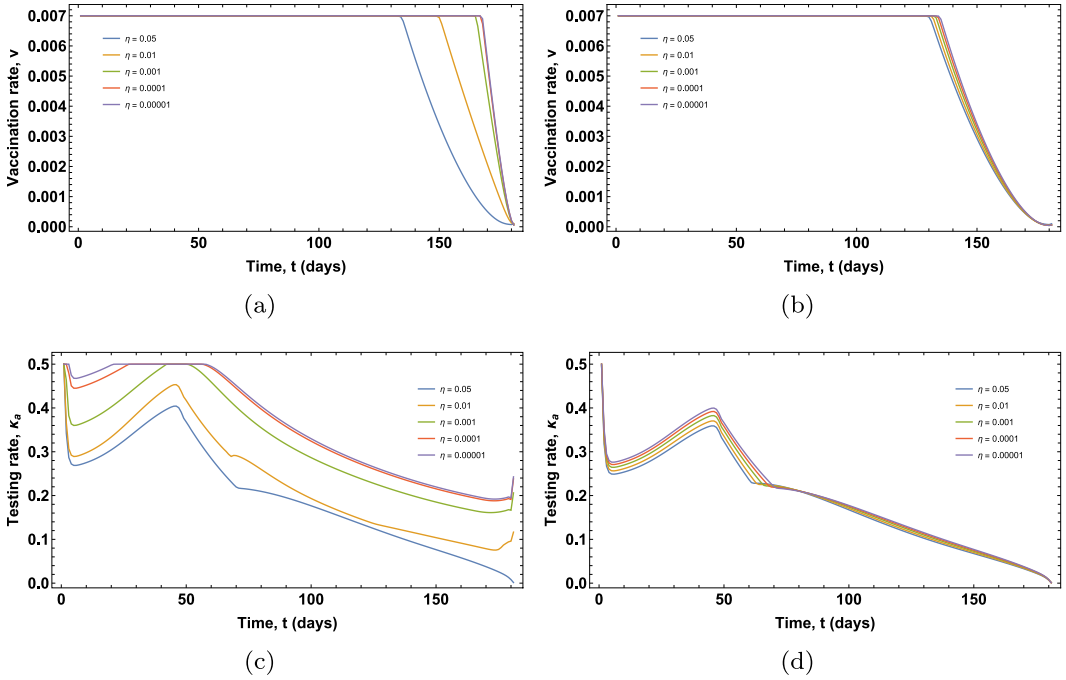

Fig. 10. Experiment B. Optimal vaccination and testing rates obtained using the CC reformulation (left) and the FMM reformulation (right) for different values of the joint risk level η.

should be carried out to rule out those random parameters that do not actually contribute to the variability of the optimal stochastic state variables.

The Sobol' indices corresponding to the optimal solutions of (18) are shown in Fig. 12. The variance of all the optimal state variables can be mainly attributed to the variance of the susceptible-infected transmission rate α, the ailing recovery rate ξ, and the threatened recovery rate σ. This is useful information that can be taken into account to alleviate the computational burden in further experiments.

6.2.2. Experiment D

In this experiment, for all $t \in [t_I, t_F]$, the chance constraint

$$P\left(T(t,\boldsymbol{\zeta}) \leq T_U\right) \geq 1 - \eta_T \tag{19}$$

has been added to the stochastic optimal control problem (18), and the resulting CCSOCP has been solved using the FMM reformulation, taking into account the results of the sensitivity analysis undertaken in Experiment C. Thus, the vector of random parameters has been set to $\boldsymbol{\zeta} = (\alpha, \xi, \sigma)$. Specifically, to mitigate the unwanted effects of the

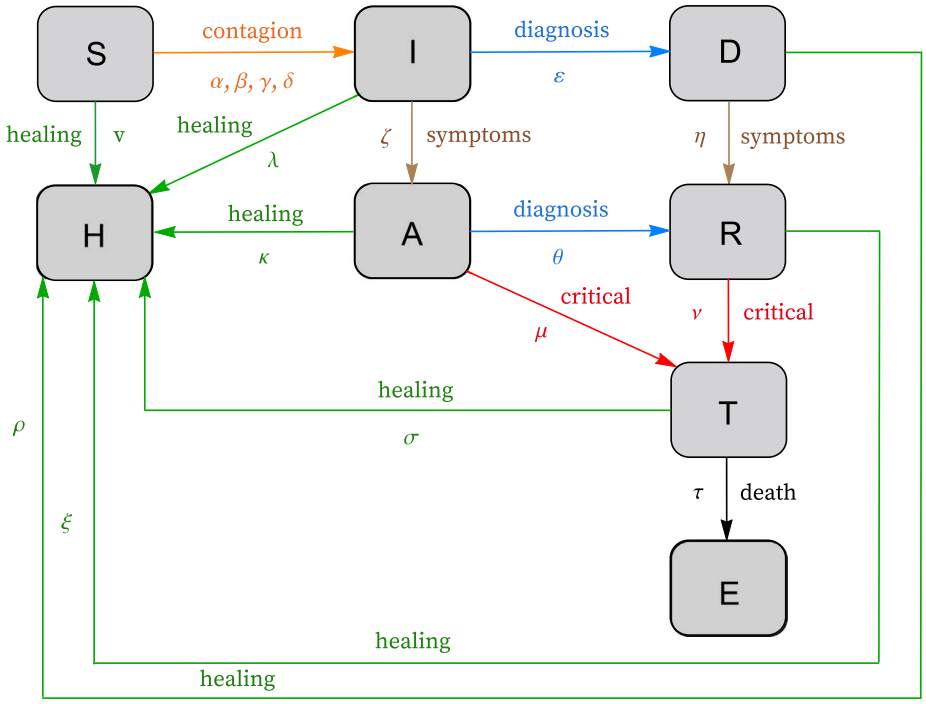

Fig. 11. Flow chart of the SIDARTHE epidemic model (18b)–(18i).

Table 4
Experiment C. Mean number of iterations (#iter), mean CPU time (CPUT), and number of quadrature weights (#QW).

	Number of random parameters, N_U								
	1	2	3	4	5	6	7	8	9
#iter	1107	5804	34 569	9745	14 319	19 853	26 251	32 798	36 980
CPUT (s)	27.73	143.16	905.80	243.95	360.51	501.19	651.59	820.04	893.46
#CW	5	25	125	45	66	91	120	153	190

disease, the upper bound on the proportion of daily threatened subjects has been set to $T_U = 0.15$ and the corresponding risk level has been set to $\eta_T = 0.05$.

Fig. 13 shows the expected values of the proportions of subjects for each optimal state variable, along with the corresponding 2-sigma confidence envelopes obtained using the FMM reformulation, which are represented in green lines. The associated deterministic optimal control variable is depicted in Fig. 14. For the sake of comparison, Figs. 13 and 14 also include the optimal solutions of the stochastic optimal control problem (18), represented in red lines, namely the optimal solutions obtained if the chance constraint (19) is not considered and assuming $\boldsymbol{\zeta} = (\alpha, \xi, \sigma)$.

As in Experiment A, the influence of the chance constraint (19) on the optimal solutions can be clearly appreciated in Fig. 13, particularly in Fig. 13.d, when compared to the optimal solutions obtained without considering such constraint. The reduction in the proportion of threatened subjects caused by constraint (19) is achieved at the expense of increasing the testing of asymptomatic subjects during the first half of the time interval, as it can be seen in Fig. 14.

7. Conclusions

A methodology for the reformulation of chance-constrained stochastic optimal control problems has been proposed with the aim of guaranteeing a dependable uncertainty management in the context of epidemic models. It relies on the so-called fourth moment method within a spectral approach, in which a reliable reformulation of the chance constraints is based on the efficient computation of the first four statistical moments of the stochastic state variables.

This approach requires the calculation of two more moments in comparison with those methods based on the Chebyshev–Cantelli's inequality. However, the surrogate models of the optimal state variables provided by the polynomial chaos spectral expansion allow these two moments to be computed at a very low extra computational cost. Moreover, the fourth moment-based approach does not present the reliability issues suffered by the methods that rely on the Chebyshev–Cantelli's inequality.

Specifically, when high accuracy is required for the risk level associated to the fulfillment of the chance constraints, the bounds provided by the Chebyshev–Cantelli's inequality are too coarse, which usually result in solutions of the epidemic chance-constrained stochastic optimal control problem that, in practice, imply the implementation of inefficient or even infeasible control strategies for the public health system.

The optimal control of two stochastic mathematical models of the COVID-19 transmission has been considered to show the practical implementation of the proposed methodology. In the numerical experiments, in which single and joint chance constraints have been considered, both reformulation approaches have been compared. The results show the presence of the reliability issues that arise when the reformulation based on the Chebyshev–Cantelli's inequality is used. In particular, as the risk level decreases, the corresponding optimal control variables provide increasingly inefficient strategies until they become practically unviable or infeasible. Conversely, the optimal control variables obtained when the fourth moment-based reformulation is employed yield strategies that behave accordingly to the required risk levels and are viable for the public health system.

Given these promising results in the framework of the COVID-19 epidemic models, an appealing line of future research would be to apply the proposed methodology to dengue fever control. Dengue, like

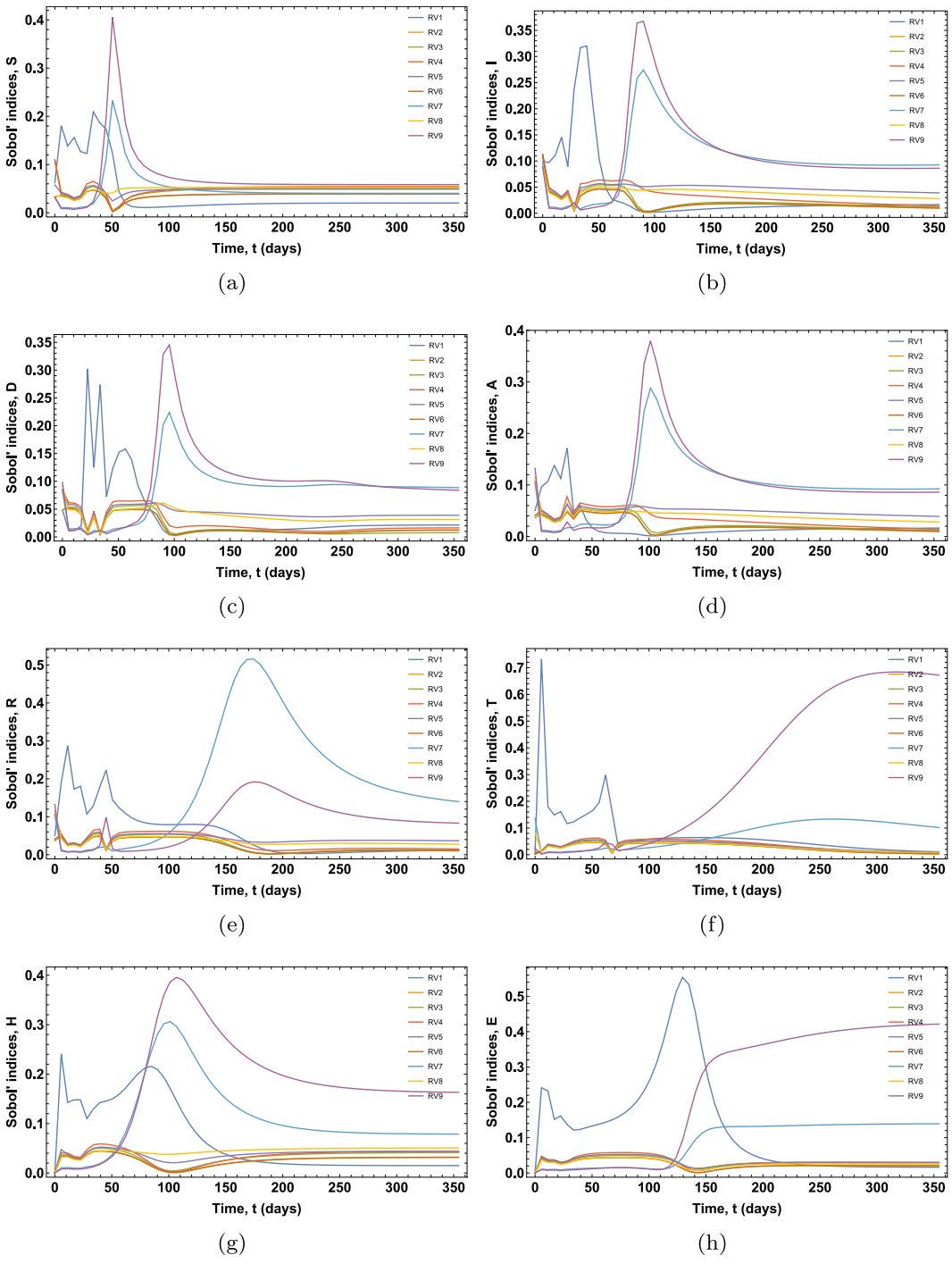

Fig. 12. Experiment C. Sobol' indices associated with the random parameters $\boldsymbol{\zeta} = (\alpha, \beta, \gamma, \delta, \lambda, \kappa, \xi, \rho, \sigma)$ in the solution of the stochastic optimal control problem (18).

COVID-19, is an infectious disease that poses significant challenges in terms of prevention and control. In fact, it is the fastest-growing infectious disease globally [31]. The application of the proposed methodology could provide new insights and tools to address these challenges, thereby enhancing dengue control strategies.

CRediT authorship contribution statement

Almudena Buelta: Writing – review & editing, Writing – original draft, Visualization, Validation, Supervision, Software, Methodology, Investigation, Formal analysis, Conceptualization. **Alberto Olivares:** Writing – review & editing, Writing – original draft, Visualization, Validation, Supervision, Software, Methodology, Investigation, Formal analysis, Conceptualization. **Ernesto Staffetti:** Writing – review & editing, Writing – original draft, Visualization, Validation, Supervision, Software, Methodology, Investigation, Formal analysis, Conceptualization.

Declaration of competing interest

The authors declare that they have no known competing financial interests or personal relationships that could have appeared to influence the work reported in this paper.

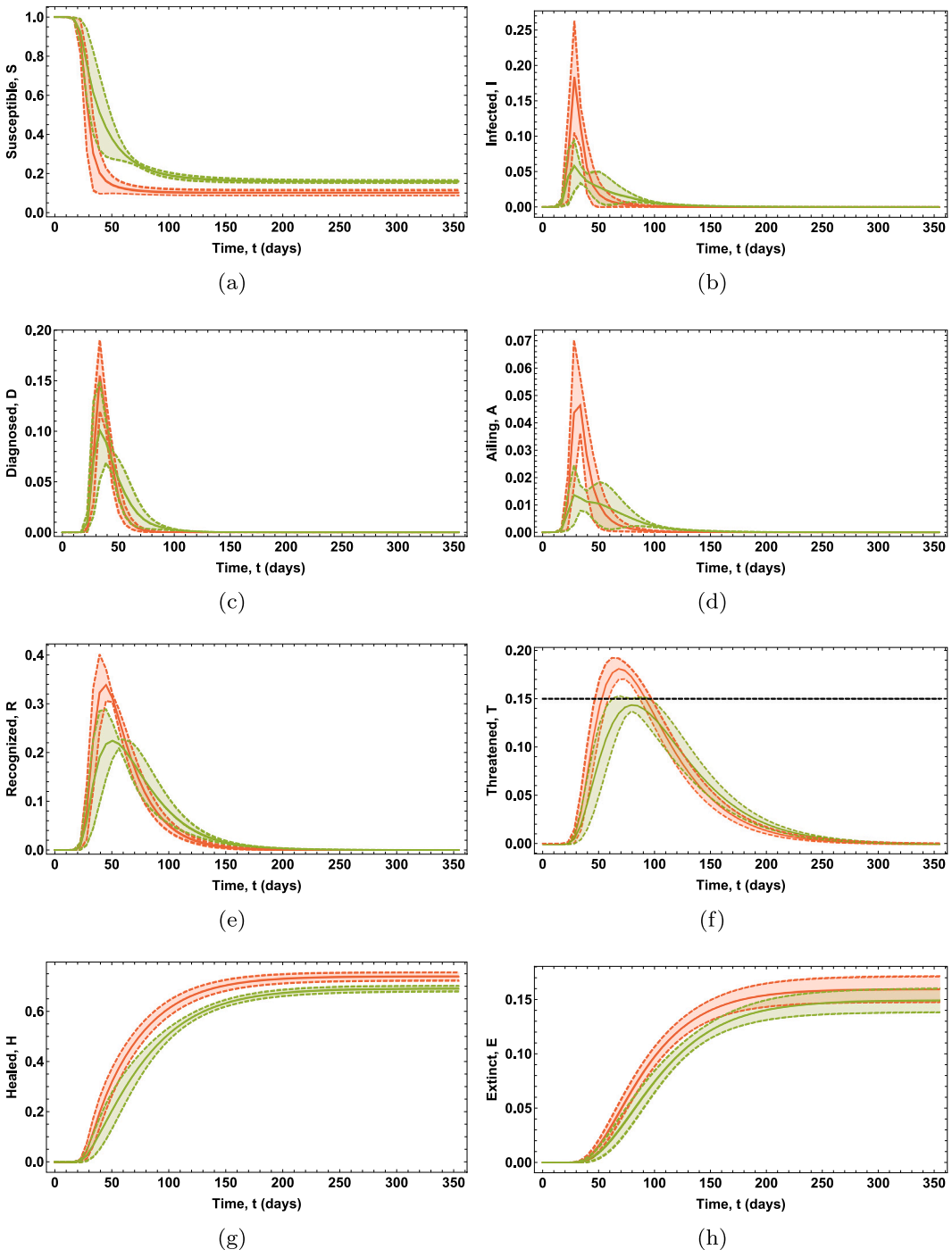

Fig. 13. Experiment D. Expected values of the proportions of subjects for each state variable, along with the corresponding 2-sigma confidence envelope. The optimal solutions obtained using the FMM reformulation are shown green. The optimal solutions obtained without chance constraint are shown in red.

Appendix A. Gaussian cubature rule

As mentioned in Section 3, to solve the integral (6), a Gaussian cubature rule based on the statistical moments of the random vector $\boldsymbol{\zeta} = (\zeta_1, \ldots, \zeta_{N_U})$ is used in this paper. Specifically, given an arbitrary multivariate function $F(\boldsymbol{\zeta})$, its full tensor product cubature can be formulated as

$$\int_{c_1}^{d_1} \cdots \int_{c_{N_U}}^{d_{N_U}} F(\boldsymbol{\zeta})\, d\mathcal{P}(\boldsymbol{\zeta}) \approx \sum_{i_1=1}^{p_1} \cdots \sum_{i_{N_U}=1}^{p_{N_U}} F\left(\zeta^{i_1}, \ldots, \zeta^{i_{N_U}}\right) \times \left(\omega_{i_1} \otimes \cdots \otimes \omega_{i_{N_U}}\right), \tag{A.1}$$

with ζ^{i_j} and $\omega_{i_j}, i = 1, \ldots, p, j = 1, \ldots, N_U$, denoting, respectively, the nodes and weights obtained from the statistical moments of the random vector $\boldsymbol{\zeta}$ [32].

Moreover, a sparse-grid cubature, such as the Smolyak cubature rule [33], can be employed instead of the tensor-grid cubature when the number of random variables N_U grows, in order to avoid the curse of dimensionality [22]. Specifically, given the random parameters ζ_i, $i = 1, \ldots, N_U$, let $\mathcal{U}^{i_j}$, $i = 1, \ldots, p, j = 1, \ldots, N_U$, denote a sequence of N_U univariate quadrature rules. That is, each of this univariate

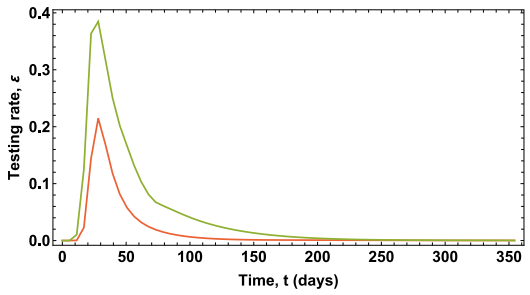

(a)

Fig. 14. Experiment D. Optimal testing rate. The optimal control obtained using the FMM reformulation is shown in green. The optimal control obtained without chance constraint is shown in red.

quadrature rules can be expressed in terms of a set of nodes and weights as

$$\mathcal{U}^{i_j} = \sum_{k=1}^{m_{i_j}} \omega_{i_j}^k F(\zeta_k^{i_j}), \tag{A.2}$$

where m_{i_j}, $j = 1, \dots, N_U$, is the maximum order for each univariate quadrature. Thus, individual orders for the random parameters are taken into account, which allows to consider an anisotropic grid if required.

Then, the Smolyak quadrature rule for multiple random parameters can be calculated as

$$\mathcal{Q}^{\iota,N_U} = \sum_{\iota+1 \le |\boldsymbol{i}| \le \iota+N_U} (\iota-1)^{\iota+N_U-|\boldsymbol{i}|} \binom{N_U-1}{\iota+N_U-|\boldsymbol{i}|} \left(\mathcal{U}^{i_1} \otimes \mathcal{U}^{i_2} \otimes \cdots \otimes \mathcal{U}^{i_{N_U}}\right) \tag{A.3}$$

with

$$|\boldsymbol{i}| = \sum_{k=1}^{N_U} \boldsymbol{i}_k = \sum_{k=1}^{N_U} \mathcal{I}_j^k,$$

where ι is the so-called level of the quadrature rule and $|\boldsymbol{i}|$ denotes the norm of the vector of indices $\boldsymbol{i} = \{i_1, i_2, \dots, i_{N_U}\}$, that is, the sum of a row j of the index matrix $\mathcal{I}_j^k$ that represents the Smolyak graded lexicographic ordering. In other words, the rows of the index matrix $\mathcal{I}_k^i$ contain which order of each univariate polynomial contributes to a particular multivariate polynomial.

The level ι in (A.3) can be considered as the order in the full Gaussian quadrature setting, that is, it controls the accuracy of the rule. Thus, for a fixed number of random parameters, increasing the level ι provides a better accuracy. For instance, the sparse Smolyak index matrix for $N_U = 3$ and $\iota = 2$ is the following

$$\mathcal{I}_{\iota+1 \le |\boldsymbol{i}| \le \iota+N_U} = \mathcal{I}_{3 \le |\boldsymbol{i}| \le 5} = \begin{bmatrix} 1 & 1 & 1 \\ 2 & 1 & 1 \\ 1 & 2 & 1 \\ 1 & 1 & 2 \\ 3 & 1 & 1 \\ 2 & 2 & 1 \\ 1 & 3 & 1 \\ 2 & 1 & 2 \\ 1 & 2 & 2 \\ 1 & 1 & 3 \end{bmatrix}.$$

The set of sparse nodes in (A.2) and (A.3) is calculated as

$$\mathcal{G}^{\iota,N_U} = \bigcup_{\iota+1 \le |\boldsymbol{i}| \le \iota+N_U} \left(\zeta^{i_1} \times \zeta^{i_2} \times \cdots \times \zeta^{i_{N_U}}\right),$$

where ζ^{i_j}, $j = 1, \dots, N_U$, represent the m_{i_j} collocation points used by the quadrature $\mathcal{U}^{i_j}$. The corresponding vector of sparse weights $\boldsymbol{\omega}_S$ is calculated as

$$\boldsymbol{\omega}_S = Q_S \cdot \left(\mathcal{W}^{i_1} \otimes \mathcal{W}^{i_2} \otimes \cdots \otimes \mathcal{W}^{i_{N_U}}\right),$$

where $\mathcal{W}^{i_j}$ is the matrix whose columns are the univariate nodes of the jth random parameter, and Q_S is the so-called Smolyak counting coefficient, which is obtained as

$$Q_S = (-1)^{N_S} \binom{N_U-1}{N_S}, \quad \text{with} \quad N_S = \iota + N_U - \sum_{i=1}^{N_U} \mathcal{I}_j^i.$$

As in the case of the full tensor quadrature (A.1), the coefficients of the corresponding multi-dimensional polynomial chaos expansion can be calculated through Smolyak sparse integration following the integral quadrature approach already described in (6), with $c_k^l(t)$, $k = 1, \dots, N_{SP}$, $l = 1, \dots, n$, being N_{SP} the number of Smolyak sparse collocation points.

Alternatively, the coefficients $c_k^l(t)$, $k = 1, \dots, N_{SP}$, $l = 1, \dots, n$, can be estimated by means of linear regression, which is specially recommended for high values of the Smolyak level ι. In particular, let $\hat{\boldsymbol{c}}^l(t) = (\hat{c}_1^l(t), \hat{c}_2^l(t), \dots, \hat{c}_{N_{SP}}^l(t))$ denote the vector of estimated coefficients. Then, $\hat{\boldsymbol{c}}^l(t)$ can be computed solving the system of linear equations

$$\left(\boldsymbol{R}_l^T \boldsymbol{R}_l\right) \hat{\boldsymbol{c}}^l(t) = \boldsymbol{R}_l^T \tilde{\mathbf{z}}_l(t),$$

where

$$\boldsymbol{R}_l = \begin{bmatrix} \boldsymbol{\Psi}_1^l(\zeta^{i_1}) & \boldsymbol{\Psi}_2^l(\zeta^{i_1}) & \cdots & \boldsymbol{\Psi}_{N_{SP}}^l(\zeta^{i_1}) \\ \boldsymbol{\Psi}_1^l(\zeta^{i_2}) & \boldsymbol{\Psi}_2^l(\zeta^{i_2}) & \cdots & \boldsymbol{\Psi}_{N_{SP}}^l(\zeta^{i_2}) \\ \vdots & \vdots & \ddots & \vdots \\ \boldsymbol{\Psi}_1^l(\zeta^{i_{N_U}}) & \boldsymbol{\Psi}_2^l(\zeta^{i_{N_U}}) & \cdots & \boldsymbol{\Psi}_{N_{SP}}^l(\zeta^{i_{N_U}}) \end{bmatrix} \quad \text{and}$$

$$\tilde{\mathbf{z}}_l(t) = \begin{bmatrix} z_l(t, \zeta^{i_1}) \\ z_l(t, \zeta^{i_2}) \\ \vdots \\ z_l(t, \zeta^{i_{N_U}}) \end{bmatrix}.$$

Appendix B. Sobol' indices computation

As mentioned in Section 4, the surrogate model provided by the polynomial expansion (5) can be employed to undertake a global sensitivity analysis, which is based on the variance of the optimal state variables $\mathbf{z}(t, \boldsymbol{\zeta})$. This sensitivity analysis relies on the computation of the Sobol' indices, which quantify how much of the variance of $\mathbf{z}(t, \boldsymbol{\zeta})$ is explained by the variance of each component of the vector of random parameters $\boldsymbol{\zeta} = (\zeta_1, \dots, \zeta_{N_U})$. To this end, $\mathbf{z}(t, \boldsymbol{\zeta})$ is assumed to be square integrable and the random parameters ζ_i, $i = 1, \dots, N_U$, are supposed to be independent. Specifically, if the full tensor product cubature is considered, the Sobol' index $S_i^l(t)$ associated to the random parameter ζ_i, $i = 1, \dots, N_U$, and the state variable $z_l(t, \boldsymbol{\zeta})$, $l = 1, \dots, n$, is computed as

$$S_i^l(t) = \frac{1}{\sigma_{z_l}^2(t)} \sum_{\mathbf{k} \in \mathcal{J}_i, \mathbf{k} \neq 0} c_k^l(t)^2, \tag{B.1}$$

where $\sigma_{z_l}^2(t)$ is the variance calculated in (7b) and $\mathcal{J}_i$ represents the set of multi-indices

$$\mathcal{J}_i = \left\{\mathbf{k} \in \mathbb{N}^{N_U} : |\mathbf{k}| \le N_P \mid k_i > 0, k_{j \neq i} = 0\right\}.$$

Otherwise, if the Smolyak cubature is used, the set $\mathcal{J}_i$ in (B.1) must be replaced by

$$\mathcal{J}_i^S = \left\{\mathbf{k} \in \mathbb{N}^{N_U} : |\mathbf{k}| \le \iota + N_U \mid k_i > 0, k_{j \neq i} = 0\right\}$$

Appendix C. Failure probability computation

As mentioned in Section 5.2, the failure probability for the performance function $G(z(t, \boldsymbol{\zeta}))$ can be also obtained using the Edgeworth expansion, as

$$P\left(G(z(t, \boldsymbol{\zeta})) \le 0\right) = \Phi(-\beta_{SM}(t)) - \Phi(\beta_{SM}(t)) \Delta_{FM}(t),$$

with

$$\Delta_{FM}(t) = \frac{1}{6} \alpha_{3G}(t) H_2(-\beta_{SM}(t)) + \frac{1}{24} \left(\alpha_{4G}(t) - 3\right) H_3(-\beta_{SM}(t))$$

$$+\frac{1}{72}\alpha_{3G}^2(t)H_5(-\beta_{SM}(t)),$$

where $H_2(\cdot)$, $H_4(\cdot)$, and $H_5(\cdot)$, respectively, denote the Hermite polynomials of second, third, and fifth order, namely

$$H_2(x) = x^2 - 1,$$
$$H_3(x) = x^3 - 3x,$$
$$H_5(x) = x^5 - 10x^3 + 15x.$$

References

[1] A. Bagchi, Optimal Control of Stochastic Systems, in: Prentice Hall International Series in Systems and Control Engineering, Prentice-Hall, 1993.

[2] D.E. Kirk, Optimal Control Theory: An Introduction, in: Dover Books on Electrical Engineering, Dover Publications, 2004.

[3] K.B. Athreya, S.N. Lahiri, Measure Theory and Probability Theory, in: Springer Texts in Statistics, Springer, 2006.

[4] D.P. Loucks, Chance Constrained and Monte Carlo Modeling, in: Public Systems Modeling. International Series in Operations Research & Management Science, vol. 318, Springer, 2022.

[5] X. Han, P.E. Kloeden, Random Ordinary Differential Equations and Their Numerical Solution, in: Probability Theory and Stochastic Modelling, vol. 85, Springer, 2017.

[6] X. Sun, B. Zhang, R. Chai, A. Tsourdos, S. Chai, UAV trajectory optimization using chance-constrained second-order cone programming, Aerosp. Sci. Technol. 121 (2022) 107283.

[7] R.E. Keil, A.T. Miller, M. Kumar, A.V. Rao, Method for solving chance constrained optimal control problems using biased kernel density estimators, Optim. Control Appl. Methods 42 (1) (2020) 330–354.

[8] P. Piprek, S. Gros, F. Holzapfel, Rare event chance-constrained optimal control using polynomial chaos and subset simulation, Processes 7 (4) (2019) 185.

[9] A. Balataa, M. Ludkovski, A. Maheshwari, J. Palczewski, Statistical learning for probability-constrained stochastic optimal control, European J. Oper. Res. 290 (2021) 640–656.

[10] B. Gopalakrishnan, A.K. Singh, K.M. Krishna, D. Manocha, Solving chance-constrained optimization under nonparametric uncertainty through Hilbert space embedding, IEEE Trans. Control Syst. Technol. 30 (2) (2021) 901–916.

[11] A.K. Dhaibana, B.K. Jabbar, An optimal control model of the spread of the COVID-19 pandemic in Iraq: Deterministic and chance-constrained model, J. Intell. Fuzzy Syst. 40 (2021) 4573–4587.

[12] F.S. Lobato, G.M. Platt, G.B. Libotte, A.J.S. Neto, Formulation and solution of an inverse reliability problem to simulate the dynamic behavior of COVID-19 pandemic, Trends Comput. Appl. Math. 22 (2021) 91–107.

[13] P. Scarabaggio, R. Carli, G. Cavone, N. Epicoco, M. Dotoli, Nonpharmaceutical stochastic optimal control strategies to mitigate the COVID-19 spread, IEEE Trans. Autom. Sci. Eng. 19 (2) (2022) 560–575.

[14] R. Wang, Q. Wang, Determination and estimation of optimal quarantine duration for infectious diseases with application to data analysis of COVID-19, Biometrics 78 (2) (2022) 691–700.

[15] A. Armaou, B. Katch, L. Russo, C. Siettos, Designing social distancing policies for the COVID-19 pandemic: A probabilistic model predictive control approach, Math. Biosci. Eng. 19 (9) (2022) 8804–8832.

[16] L. Thul, W. Powell, Stochastic optimization for vaccine and testing kit allocation for the COVID-19 pandemic, European J. Oper. Res. 304 (3) (2023) 325–338.

[17] A. Olivares, E. Staffetti, A statistical moment-based spectral approach to the chance-constrained stochastic optimal control of epidemic models, Chaos Solitons Fractals 172 (2023) 113560.

[18] Y.-G. Zhao, T. Ono, Moment methods for structural reliability, Struct. Saf. 23 (2001) 47–75.

[19] A. Olivares, E. Staffetti, Optimal control-based vaccination and testing strategies for COVID-19, Comput. Methods Programs Biomed. 211 (2021) 106411.

[20] S. Zymler, D. Kuhn, B. Rustem, Distributionally robust joint chance constraints with second-order moment information, Math. Program. 137 (1–2) (2013) 167–198.

[21] S. Oladyshkin, W. Nowak, Data-driven uncertainty quantification using the arbitrary polynomial chaos expansion, Reliab. Eng. Syst. Saf. 106 (2012) 179–190.

[22] D. Xiu, Numerical Methods for Stochastic Computations. A Spectral Method Approach, Princeton University Press, 2010.

[23] R. Ahlfeld, B. Belkouchi, F. Montomoli, SAMBA: Sparse approximation of moment-based arbitrary polynomial chaos, J. Comput. Phys. 320 (529) (2016) 1–16.

[24] A. Trucchia, V. Egorova, G. Pagnini, M. Rochoux, On the merits of sparse surrogates for global sensitivity analysis of multi-scale nonlinear problems: Application to turbulence and fire-spotting model in wildland fire simulators, Commun. Nonlinear Sci. Numer. Simul. 73 (2019) 120–145.

[25] S.H.R. Hajiagha, S.S. Hashemi, H.A. Mahdiraji, J. Azaddel, Multi-period data envelopment analysis based on Chebyshev inequality bounds, Expert Syst. Appl. 42 (2015) 7759–7767.

[26] G. Calafiore, L. El-Ghaoui, On distributionally robust chance-constrained linear programs, J. Optim. Theory Appl. 130 (2006) 1–22.

[27] J.E. Kolassa, Series Approximation Methods in Statistics, third ed., in: Lecture Notes in Statistics, vol. 88, Springer, New York, 2006.

[28] A.L. Herman, B.A. Conway, Direct optimization using collocation based on high-order Gauss-Lobatto quadrature rules, J. Guid. Control Dyn. 19 (3) (1996) 592–599.

[29] G. Giordano, F. Blanchini, R. Bruno, P. Colaneri, A. Di Filippo, A. Di Matteo, M. Colaneri, Modelling the COVID-19 epidemic and implementation of population-wide interventions in Italy, Nat. Med. 26 (2020) 855–860.

[30] A. Olivares, E. Staffetti, Uncertainty quantification of a mathematical model of COVID-19 transmission dynamics with mass vaccination strategy, Chaos Solitons Fractals 146 (2021) 110895.

[31] S. Suchanti, B.J. Stephen, T.P. Chaurasia, A.P. Raghuwanshi, G. Singh, A. Singh, R. Mishra, *In-Silico* CLEC5A mRNA expression analysis to predict dengue susceptibility in cancer patients, Biochem. Biophys. Rep. 35 (2023) 101501.

[32] A. Olivares, E. Staffetti, Robust optimal control of compartmental models in epidemiology: Application to the COVID-19 pandemic, Commun. Nonlinear Sci. Numer. Simul. 111 (2022) 106509.

[33] K.L. Judd, L. Maliar, S. Maliar, R. Valero, Smolyak method for solving dynamic economic models: Lagrange interpolation, anisotropic grid and adaptive domain, J. Econom. Dynam. Control 44 (2014) 92–123.